Environmental Science

AIMS Environmental Science, 10(3): 424–445.
DOI: 10.3934/environsci.2023024
Received: 14 February 2023
Revised: 01 April 2023
Accepted: 03 May 2023
Published: 17 May 2023

http://www.aimspress.com/journal/environmental

Research article

Decolorization of Reactive Red 120 by a novel bacterial consortium: Kinetics and heavy metal inhibition study

Motharasan Manogaran[1], Mohd Izuan Effendi Halmi[2], Ahmad Razi Othman[3], Nur Adeela Yasid[1], Baskaran Gunasekaran[4] and Mohd Yunus Abd Shukor[1,*]

[1] Department of Biochemistry, Faculty of Biotechnology and Biomolecular Sciences, Universiti Putra Malaysia, 43400 UPM Serdang, Selangor D.E., Malaysia
[2] Department of Land Management, Faculty of Agriculture, Universiti Putra Malaysia, 43400 UPM Serdang, Selangor D.E., Malaysia
[3] Department of Chemical and Process Engineering, Faculty of Engineering and Built Environment, Universiti Kebangsaan Malaysia,43600 UKM, Bangi, Selangor D.E., Malaysia
[4] Faculty of Applied Sciences, UCSI University Kuala Lumpur (South Wing), No.1, Jalan Menara Gading, UCSI Heights 56000 Cheras, Kuala Lumpur, Malaysia

* **Correspondence:** mohdyunus@upm.edu.my; Tel: +60397696722; Fax: +60389430913.

Abstract: Juru River is one of the most polluted rivers in Malaysia. A dye-degrading bacterial consortium has been isolated from the river's sediment. This consortium JR3 consists of *Pseudomonas aeruginosa* MM01, *Enterobacter* sp. MM05 and *Serratia marcescens* MM06, which were able to decolorize up to 700 ppm of the Reactive Red 120 (RR120) dye under optimal conditions with limited substrate available. Substrate inhibition kinetics were investigated, and, based on the best model, Aiba, the maximum growth rate was 0.795 h^{-1}, while the saturation constant and inhibitory constant were 0.185% and 0.14%, respectively. In addition, the influence of various metal ions on the growth and decolorization rate of this bacterial consortium on RR120 was investigated. Chromium showed the weakest effect on the decolorization of 200 ppm RR120, with 73.5% removal and bacterial growth of 11.461 log CFU mL^{-1}. Zinc yielded the second weakest effect, followed by silver and lead, with percentages of RR120 decolorization of 63.8%, 54.6% and 50.5%, respectively. Meanwhile, cadmium, arsenic and copper reduced the decolorization of RR120 in consortium JR3 by half. Mercury strongly inhibited decolorization by 32.5%. Based on the least inhibited heavy metal in RR120 decolorization activity of consortium JR3, the best inhibitory kinetic model was Levenspiel, with a maximum growth rate of 0.632 h^{-1}, while the saturation constant and inhibitory constants were 15.08% and 0.5783%, respectively. The metal-tolerant azo dye-degrading bacterial consortium will be very useful in dye remediation in metal-laden polluted environments.

Keywords: Reactive Red 120; Bacterial consortium; biodegradation; heavy metals; kinetics

1. Introduction

Dye or colorants were traditionally made from natural ingredients such as henna, cochineal, saffron, logwood and madder root, which are derived from plants, animals and mineral rocks [1,2]. The majority of these naturally derived dyes are mordants, which require a fixing agent to retain their color. Yellow was produced by liquids extracted from various plants, brown by Mediterranean mollusk extract, indigo by *Indigofera* and purple by the *Murex* snail [3]. Because there are no fixing agents to strongly bind natural dyes to fabrics, the routine of washing and drying them tends to cause them to lose color [4]. Meanwhile, ultraviolet (UV) rays from sunlight are known to fade color because they easily break down chemical bonds in natural dyes [5].

These drawbacks gave rise to synthetic dyes that lasted much longer than natural dyes. Dyes are classified based on their chemical structure, which can be further subdivided into natural and synthetic groups, which include inorganic and organic compounds. Acidic, basic, directed, dispersed, reactive, solvent, sulfur, and vat dyes are eight classes of dyes. The azo dye family is the most established of the synthetic dyes and is widely used across all industries [6]. One or more -N=N- groups make up the aromatic compounds known as azo dyes [7,8]. The azo function is frequently covalently bonded to an aromatic ring, yielding an aromatic amine (arylamine) upon oxidation or reduction [9]. Azo dyes give bright, high-intensity pigments compared to anthraquinones. It has reasonable fastness properties, but is average compared to the carbonyl and phthalocyanine classes. The biggest advantage of azo dyes is their cost-effectiveness, which is due to the processes involved in synthesizing it. Seventy percent of the 9.9 million tons of industrial dye used annually, worth USD 30.42 billion, are azo dyes [10,11]. The supply of dyes and pigments is increasing at a pace of 3.5% per year due to the ever-increasing demand [12]. The majority of synthetic dyes, which find widespread application in the textile, paper, food, printing, cosmetic and leather sectors, are based on azo compounds [11].

Due to their inexpensive price, simple preparation, fastness, variety and intensity of color, azo dyes are widely utilized in the textile industry [13]. As an example, certain azo dyes have chemical groups with a strong affinity for metals [14]. Chromium and copper are the most common metals used in these dyes, as metal ions provide better binding with fiber, improving the resistance of the dye to washing. Because of these augmented characteristics, the material is extremely chemically, biologically and photocatalytically stable. Nonetheless, they degrade poorly in the natural setting because they are resistant to breakdown from natural causes such as light exposure, water, detergents and microorganisms [15].

In the remediation of azo dyes, the effects of heavy metals need to be investigated for the successful deployment of bioremediation. There will be little to no use if the obtained bacteria or consortium is unable to decolorize azo dyes in the presence of various heavy metals, despite establishing a high decolorization rate in a controlled environment [16]. The inhibitory effect of a substrate on the growth or degradation rate of xenobiotics can be mathematically modeled using models such as the Yano, Aiba, Haldane, Tessier-Edward and Monod models, while the inhibitory effects of metal ions on the growth or degradation rate of xenobiotics can be mathematically modeled using models such as the modified Han-Levenspiel, Wang, Liu, modified Andrews and Shukor models. The effect of the substrate on the growth or degradation rate yields important parameters, such as the

maximum growth or degradation rate and maximum tolerable substrate concentrations before complete inhibition is observed. Similarly, the effects of metal ions on the growth or degradation rate can yield parameters such as the maximum growth or degradation rate and maximum tolerable metal ion concentration before complete inhibition is observed.

In this study, the inhibitory effects of the substrate Reactive Red 120 (RR120) and the effects of several heavy metals on the decolorization rate of RR120 by a previously isolated consortium, JR3 (*Pseudomonas aeruginosa* MM01, *Enterobacter* sp. MM05 and *Serratia marcescens* MM06), are the targets of this study. This consortium, isolated from an industrial waste site in Malaysia's Juru River, was able to consume RR120 as the sole carbon source in the presence of limited co-substrate available, resulting in a metabolite that was far safer than the parent compounds themselves [17]. Because the majority of industrial dye waste effluents contain heavy metals, the consortium's ability to continuously decolorize RR120 under toxic conditions was investigated further. The concentrations of heavy metals found to have the least impact on the decolorization rate were studied further using various heavy metals' inhibition kinetics to obtain valuable inhibitory parameters. To the best of our knowledge, this is the first study on the use of metal inhibition kinetic models to probe for the quantitative effects of metal ions on the rate of RR120 dye decolorization by a bacterial consortium in the presence of various heavy metals.

2. Materials and methods

2.1. Chemicals and equipment

Acetate and Tris buffer reagents were obtained from Merck KGaA, Germany. The azo dye, RR120 (Cas No. 61951-82-4) (Table 1) was purchased from Sigma Aldrich, CO, USA. Other chemicals are of analytical grade unless stated otherwise.

Table 1. Some characteristics of the investigated dye.

Properties	Reactive Red 120
Colour index name	Reactive Red-120 (RR120)
Molecular formula	$C_{44}H_{24}C_{12}N_{14}Na_6O_{20}S_6$
Molecular weight	1469.34 g/mol
Water solubility	70 g L^{-1}
Class	Diazo (-N=N-)

2.2. Preparation of bacterial inoculum

A total of three strains from consortium JR3 were used in this study. They were identified as *Enterobacter* sp. MM05, *Pseudomonas aeruginosa* MM01 and *Serratia marcescens* MM06, which were previously isolated from Juru River, Malaysia [17]. Large-scale cultures of each strain were grown in a sterile medium containing 10 g L^{-1} of nutrient broth and 2 g L^{-1} of yeast extract to promote rapid bacterial growth development. Adjustment of the medium to pH 7.0 was carried out using 1 M HCl or 1 M NaOH. Each strain was individually inoculated into a 1-L growth medium separated into several conical flasks. Growth of the bacterium was carried out on an orbital shaker at 120 rpm and room temperature. The bacterial cells were harvested by centrifuging at 10,000 × g at the exponential phase (18 h±2) at the temperature of 4 °C for 10 min. The resulting pellets were washed twice using

100 mM Tris buffer and then re-suspended in pH 7 Tris buffer solution to an A600 nm range of 0.9 – 1.0. Additionally, 100 µL from each of the washed cells was mixed to get a final volume of 1 mL or 1%. This was done to standardize the inoculum size.

2.3. Analytical methods

Dye solutions and dye-containing culture media were filtered and sterilized with a Millipore Millex© GS 0.22-µm unit. The dye concentrations were measured using a UV-visible spectrophotometer that had been calibrated to the specified maximum wavelengths of each dye (Shimadzu UV mini 1240). Each of the samples was centrifuged for 10 min at 10,000 × g using a Beckman Coulter© Microfuge 16 centrifuge. The concentration of the dye was evaluated as follows.

$$\%Decolorization = \frac{initialabsorbance - finalabsorbance}{initialabsorbance} \times 100 \quad (1)$$

Enumeration of the bacteria was carried out using the colony-forming unit (CFU mL^{-1}) with appropriate dilutions.

2.4. Effects of various Reactive Red 120 concentrations on decolorization ability and growth rate of consortium JR3

Based on previously obtained RSM results, consortium JR3 was inoculated under optimal conditions for maximum decolorization of RR120 at various concentrations [17]. A total of 1 mL of seed culture consortium JR3 was inoculated in 100 mL of minimal salts medium (MSM) containing different concentrations of RR120, and it was incubated under shaking conditions (150 rpm) for five days. The composition of MSM in (g L^{-1}) of dH_2O comprised $Na_2HPO_4.2H_2O$ (12.0), KH_2PO_4 (2.0), $MgCl_2.6H_2O$ (0.10), $Ca(NO_3)_2.4H_20$ (0.050) and $FeCl_2.4H_20$ (0.0075), while the trace elements (mg L^{-1}) were $ZnCl_3$ (50), $MnCl_2.4H_2O$ (30), $CoCl_2.6H_2O$ (200), $NiC_{l2}.6H_2O$ (20), $Na_2MoO_4.2H_2O$ (30), H_3BO_3 (300) and $CuCl_2.2H_2O$ (10) [18]. The concentration of $NH_4(SO_4)_2$ and the pH varied depending on the RR120 concentration used, as illustrated in Table 2. Yeast extract was given at a final concentration of 0.5 g L^{-1}. Each concentration of RR120 was experimentally designed based on Table 2 for maximum decolorization ability by consortium JR3, resulting in peak performance. Reading was taken at an interval of 3 h for the first 24 h, followed by a 12-h interval for the remaining incubation period. Decolorization of RR120 was determined against the medium as a blank at 525 nm.

Table 2. Suggested parameters for each variable for optimum decolorization of RR120 by consortium JR3 based on response surface methodology optimization.

No.	Ammonium sulphate concentration (g L^{-1})	pH	Temperature (°C)	RR120 concentration (ppm)	Desirability
1.	0.6	8.102	34.233	25	0.999
2.	0.6	8.102	34.233	50	0.999
3.	0.6	8.102	34.233	100	0.999
4.	0.645	8.293	34.532	200	1.000
5.	0.681	8.527	33.717	300	0.999
6.	0.702	8.555	33.502	400	0.999
7.	0.711	8.629	33.121	500	0.999
8.	0.822	8.874	31.687	600	0.999
10.	0.841	8.743	28.971	700	0.999

2.5. Primary modeling of Reactive Red 120 decolorization

The Gompertz model was used to calculate specific reduction rates and lag times. This was done initially to determine the specific rate of reduction for each concentration; these are important parameters to have before moving on to secondary modeling. The bacterial growth rate on RR120 data was first converted to a natural logarithm before being used with the modified Gompertz model, which is commonly used in bacterial kinetics [19–24].
The equation is as follows:

$$\ln\left(\frac{X}{Xo}\right) = \ln\left(\frac{Xmax}{Xo}\right)\exp\left(-\exp\left(\frac{\mu m.e}{\ln\left(\frac{Xmax}{Xo}\right)}(\lambda - t) + 1\right)\right) \quad (2)$$

where
X_0 is the initial bacterial concentration (CFU mL^{-1}),
X_{max} is the maximum initial bacterial concentration (CFU mL^{-1}),
X is the bacterial concentration (CFU mL^{-1}),
t is the incubation time (h),
μ_m is the maximum specific growth rate (h^{-1}),
λ is the lag time (h)

2.6. Secondary modeling of Reactive Red 120 decolorization

For primary growth kinetics, an increase in bacterial number (CFU) over time was performed while fitting the resultant specific growth rate; meanwhile, primary growth activity against RR120 concentration represents secondary growth modeling. When fitting the graph, the Marquardt algorithm was used, which minimizes the residual sums of squares (i.e., the difference between predicted and observed). CurveExpert Professional software (version 2.0) was used to fit curves for both primary and secondary growth graph models. The terms are as follows:

i. Estimation of μ_{max}: The maximal bacterial growth rate is an important parameter for modeling microbial growth under batch conditions. Each formula has its way of calculating μ_{max} which depends on the interaction of the substrate concentration and bacteria tolerance level. Therefore,

six different estimation methods were used to find the ideal μ_{max}. The estimation was carried out by utilizing the steepest ascent search of the curve among four datum points.

ii. Estimation of λ : In this study, a stochastic model is used to investigate the lag distribution of consortium JR3 for various RR120 concentrations. It was accomplished by determining the intersection of points 1 (0 h) and *x* (start of the exponential phase). To plot the graph, a minimum of six points were obtained during the lag phase.

iii. Estimation of *A*: The maximum amount of bacterial growth was carried out by taking the final datum point at the highest peak.

Table 3. Models used to model secondary inhibition kinetics using consortium JR3 on various concentrations of RR120 under optimized conditions.

Models	Equation	Authors
Yano	$\frac{\mu_{max} S}{S + K_s + \left(\frac{S^2}{K_1}\right)\left(1 + \frac{S}{K}\right)}$	[25]
Aiba	$\mu_{max} \frac{S}{K_s + S} exp(-KP)$	[26]
Haldane	$\mu_{max} \frac{S}{S + K_s + \frac{S^2}{K_i}}$	[27]
Tessier-Edward	$\mu_{max}(1 - \exp\left(\frac{S}{K_i}\right) - exp\left(\frac{S}{K_s}\right)$	[28]
Monod	$\mu_{max} \frac{S}{K_s + S}$	[29]

Notes: Where

μ_{max} is the maximal growth rate (h^{-1})

K_S is the half-saturation constant for maximal reduction (mg/L)

S_m is the maximal concentration of substrate tolerated (mg/L)

m, n, K are curve parameters

S is the substrate concentration (mg/L)

P is the product concentration (mg/L)

2.7. Effects of heavy metals on Re (mg/L) *active Red 120 decolorization by consortium JR3*

In this study, we looked at how well consortium JR3 could remove colour from 200 ppm RR120 under ideal conditions while still dealing with heavy metals. The heavy metals used in this study were silver, arsenic, chromium, cadmium, copper, lead, mercury and zinc. MERCK AAS standard solution was used to prepare each heavy metal stock, and 1 ppm of the prepared stock was then added to the culture media. During the incubation process, the culture medium was shaken (150 rpm). At 525 nm, the absorbance of RR120 decolorization was measured.

2.8. Effects of chromium and mercury on the decolorization of Reactive Red 120 by consortium JR3

Based on Section 2.5, the chromium that had the weakest effect on the decolorization of RR120 by the consortium JR3 was studied at higher concentrations. Filter sterilized chromium (200 ppm stock solution) was supplemented to the MSM at the final concentrations of 1, 1.5, 3, 5, 7, 10, 12 and 15

ppm. Readings were taken at 12-h intervals. In the meantime, mercury, which showed a strong inhibitory effect on the decolorization of RR120 by consortium JR3, was also studied at higher concentrations. Filter sterilized mercury from a stock solution of 10 ppm were added into the MSM at the final concentrations of 0.1, 0.3, 0.5, 0.7 and 0.9 ppm. Readings were taken at 12-h intervals.

2.9. Inhibition kinetics of heavy metal on RR120 decolorization by consortium JR3

The initial study based on Section 2.7 illustrated that chromium results in the weakest effect on the decolorization ability of consortium JR3; hence, differences in increased concentration of chromium of up to 10 ppm were used to investigate the inhibition rate. The seed culture was incubated in 100 mL of MSM containing 200 ppm RR120 with different concentrations of chromium (0, 1, 1.5, 3, 5, 7, 10 and 12 ppm). The culture was incubated under shaking conditions, and the absorbance reading was taken at an interval of 3 h for the first 12 h, followed by 24-h intervals until 72 h. The values of the specific RR120 reduction rate coefficient μ at each initial chromium concentration were obtained by plotting ln (μ decolorization) vs. time. A nonlinear curve was obtained by plotting against metal concentrations; the modeling could be done to determine the constants based on Table 4. A no-lag-phase Gompertz model was employed for primary kinetics to determine each chromium concentration's μ_{max} value. During the secondary model, the inhibitory kinetics on RR120 reduction was calculated using the specific reduction rate obtained from the no-lag-phase Gompertz model in primary modeling. The models in Table 4 were used to obtain the lowest K_s (half-saturation constant) and K_i (inhibition constant).

Table 4. Metal inhibition kinetics used to model in consortium JR3.

Models	Equation	Author
Modified Han-Levenspiel	$r = u_{max}\left(1 - \frac{C}{C_{crit}}\right)^m$	[30]
Wang	$r = \frac{u_{max}}{1 + \left(\frac{C}{K_C}\right)^m}$	[31]
Liu	$r = \frac{u_{max}K_C}{K_C + C}$	[32]
Modified Andrews	$r = \frac{u_{max}C}{K_s + C + \left(\frac{C^2}{K_i}\right)}$	[33]
Shukor	$r = v_{max}\left(1 - \left(\frac{C}{S_m}\right)^n\right)$	[34]

2.10. Statistical analysis

The corrected Akaike information criterion (AICc), The root-mean-square Error (RMSE), the adjusted coefficient of determination (R^2), the bias factor (BF) and the accuracy factor (AF) were the error functions utilized in this study to discover which model is the best. The variables of the RMSE equation below are *n*, which is the number of experimental data, Ob_i, that denotes the observed or

experimental data, Pd_i is the predicted data and p is the number of parameters assessed by the model [35].

$$RMSE = \sqrt{\frac{\sum_{i=1}^{n}(Pd_i - Ob_i)^2}{n-p}} \tag{3}$$

In linear regression, the best-fitting model is determined by R^2, or the coefficient of determination. However, in nonlinear regression, R^2 does not give a comparative analysis where the number of parameters between models is different. To overcome this, the adjusted R^2 was used to calculate the closeness of the feature of the nonlinear models to unity. In the adjusted R^2 formula, S_y^2 is the total variance of the *y* variable, and RSS is the residual sum of square

$$Adjusted(R^2) = 1 - \frac{RSS}{S_Y^2} \tag{4}$$

$$Adjusted(R^2) = 1 - \frac{(1-R^2)(n-1)}{(n-p-1)} \tag{5}$$

The Akaike information criterion (AIC) provides a method to select a model for the relative quality of a given statistical model in a given set of experimental data. However, the AICc is used for data sets with a large number of parameter or those that have a smaller number of values [36]. For each data set, the AICc was calculated based on the following equation:

$$AICc = 2p + n1n\left(\frac{RSS}{n}\right) + 2(p+1) + \frac{2(p+1)(p+2)}{n-p-2} \tag{6}$$

Here, *n* indicates the number of experimental points and *p* denotes the number of parameters in the model. The AICc provides information about the variations in the number of parameters and the fitting between two models. The smallest AICc value would indicate the best fit between the models [36].

To test the goodness of fit of the models used, the BF and AF were used. In a molybdenum reduction, the BF should be equal to 1 to provide an ideal match between the observed and predicted values. The value of the BF that is greater than 1 signifies a fail-safe model, and a BF less than 1 signifies a fail-negative model. A value of AF that is ≥ 1 signifies a less precise prediction.

$$Biasfactor = 10\left(\sum_{i=1}^{n} log\frac{(Pd_i/Ob_i)}{n}\right) \tag{7}$$

$$Accuracyfactor = 10 \tag{8}$$

3. Results

3.1. Effect of initial Reactive Red 120 concentration on the growth of the consortium

RR120 growth kinetics was determined by measuring the cell growth rate at different RR120 concentrations for 72 h, as shown in Figure 1. The primary growth model was constructed based on the modified Gompertz model. This was done initially to obtain the μ_{max} value for each concentration, which is required before secondary modeling [37,38]. From 25 ppm to 700 ppm of RR120, the

consortium reached an exponential growth rate at 24 h of incubation. The consortium reached the highest growth rate at 200 ppm, and then it started to decrease with an increase in RR120 concentration. As shown in Figure 1, a high RR120 concentration above 200 ppm had a negative effect on the consortium growth rate. The highest cell growth was observed at 200 ppm with 26.1 ln CFU mL^{-1} at 48 h, followed by 100 ppm with 25.9 ln CFU mL^{-1}. Meanwhile, the concentration of RR120 resulted in better cell growth of the consortium at 50, 100, 200 and 300 ppm, as compared to 25 ppm alone. Beyond 400 ppm, the increasing concentration of RR120 significantly inhibits the consortium growth rate. For instance, at 700 ppm, the growth rate reached a plateau at 36 h with 21.5 ln CFU mL^{-1}. In comparison with 200 ppm, 700 ppm reduced the consortium growth by 74.72% at 36 h.

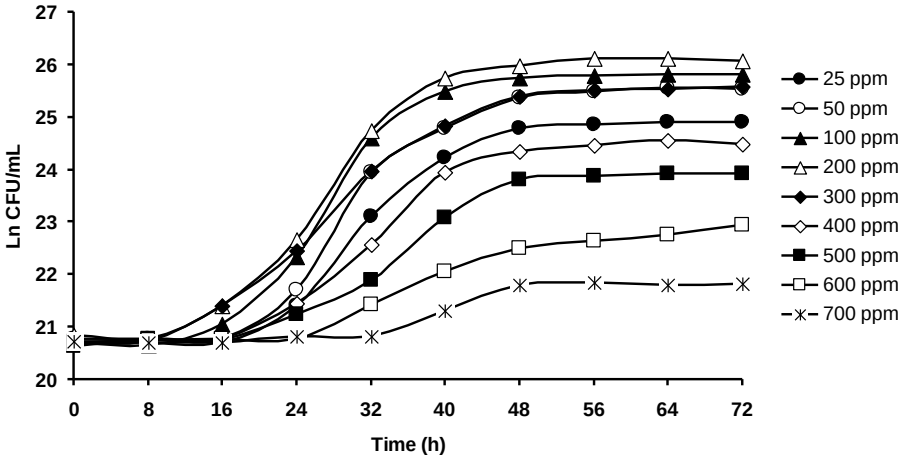

Figure 1. Effects of various RR120 dye concentrations on consortium growth rate. Data points represent mean ± SD.

3.2. Secondary modeling of consortium JR3 on the various concentrations of Reactive Red 120

The model's fitness in terms of envisaging the rate of decolorization (*q*) is illustrated in Figure 2. The correlation coefficient value for the RR120 inhibition Aiba model was 0.9939, illustrating a good fit, while the Yano model gave a slightly lower value of 0.9799. The low correlation coefficient value of 0.1986 indicates a poor fit (Table 5).

R^2 in statistics plays a major role in giving information about the goodness of fit of a model. In regression, the determination of R^2 is a statistical measure of how precise regression predictions are estimated against the real data points. Therefore, an R^2 value of 1 indicates that the regression prediction model perfectly fits the data. However, when modeling with nonlinear regression, this method does not consider the number of parameters of models and, therefore, does not freely provide comparative analysis. As a solution, when building the nonlinear models, the adjusted R^2 was utilized, as it is calculated based on the number of parameters of models used to work out the quality of nonlinear models. The adjusted coefficient of determination for Aiba was 0.983, followed by the Yano model with 0.952. The adjusted R^2 value did not deviate much from R^2, indicating a precise model.

The BF is another good indicator for allocating the perfect match between predicted and experimental values. When dealing with microbial growth kinetics, a BF value of <1 represents a fail-dangerous model, while a value of >1 indicates a fail-safe model [39]. The AF should be ≥1, and any higher value indicates a fail-safe model. Based on these requirements, only Aiba fits a perfect model,

with a BF value of 1.006 and an AF value of 1.008. The rest of the models consist of fluctuating values, indicating a worse-fit model.

The results of curve-fitting by both the primary and secondary models were compared by using the AIC, which is based on an in-sample fit (goodness of fit). The AIC was developed by Akaike to estimate the likelihood of a model to predict future values [40]. The corrected version, AICc, was utilized by considering that the size of the data set within this study was small. A lower AICc value is more desired, as a higher value often indicates a less preferrable model. Therefore, only the Aiba model had the best AICc value of –71.65, followed by the Yano model with –55.42.

The value of the specific growth rate μ tends to increase to its optimal substrate concentration before it finally decreases at higher concentrations due to substrate inhibition. According to the best model, Aiba recorded the maximum growth rate (μ_{max}) to be 0.795 h^{-1}, while the saturation constants, also known as the half-velocity constant K and inhibitory constant K_i, were 0.185% and 0.14%, respectively.

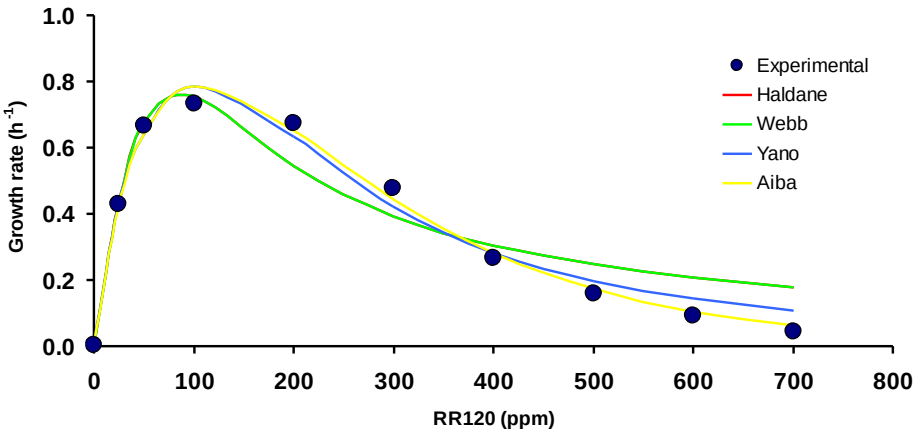

Figure 2. Growth rate on RR120 by consortium JR3, as modeled with various substrate inhibition kinetic models.

Table 5. Statistical analysis of the kinetics models for consortium JR3. adR2: adjusted R^2.

Model	*p*	RMSE	R^2	adR^2	AICc	BF	AF
Moser	4	0.256	–0.322	–1.643	–26.31	0.975	1.382
Yano	4	0.053	0.976	0.952	–55.42	1.012	1.062
Tessier-Edward	3	0.073	0.925	0.880	–50.23	1.016	1.105
Aiba	3	0.033	0.989	0.983	–71.65	1.006	1.008
Haldane	3	0.089	0.900	0.839	–45.05	1.026	1.121
Monod	2	0.243	–1.320	–2.093	–26.99	0.947	1.436

3.3. Effects of heavy metals on Reactive Red 120 decolorization by consortium JR3

The effects of heavy metals were examined for consortium JR3 to establish its ability to remediate RR120. The heavy metals used in these studies range from the highest toxic to the lowest toxic elements. Chromium showed the weakest effect on the decolorization of RR120, with 73.5% removal with bacterial growth of 11.461 log CFU (Figure 3). Zinc had the second weakest effect, followed by silver and lead, with percentages of RR120 decolorization of 63.8%, 54.6% and 50.5%, respectively.

Meanwhile, cadmium, arsenic and copper reduced the decolorization of RR120 in consortium JR3 by half. Mercury strongly inhibited decolorization by 32.5%.

3.4. Effect of mercury on the decolorization of Reactive Red 120 by consortium JR3

Mercury has a profound effect on bacterial consortium activity, as it significantly reduced the decolorization of RR120 in consortium JR3. Since consortium JR3 was isolated from the Juru River site, the effects of different concentrations of mercury on the decolorization of RR120 was investigated. Figure 4 illustrates the effects of different mercury concentrations on the decolorization of 200 ppm of RR120 and its consortium JR3 growth. The control is the condition of no mercury introduced to the media (0 ppm). Increasing the mercury concentration results in a decrease in the decolorization and bacterial growth ability of consortium JR3, where a concentration of 1.6 ppm results in total inhibition (Figure 4). At 0.1 ppm, no significant reduction in decolorization was observed, compared to the control. However, increasing the concentration beyond 0.2 ppm resulted in a significant drop in decolorization (P<0.05), and consortium JR3 lost 50% decolorization capability at 0.4 ppm of mercury. Consortium JR3 was able to tolerate the highest concentration of 1.2 ppm of mercury, with decolorization of 13.4% and bacterial growth of 10.1 log CFU mL^{-1}.

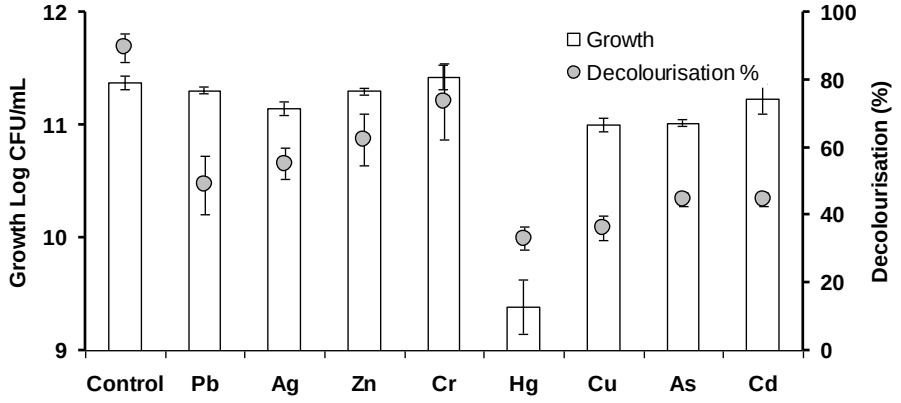

Figure 3. Growth and biodegradation effect of different heavy metals on the decolorization of 200 ppm of RR 120 by consortium JR3 after 24 h of incubation. Data points represent mean ± SD, n=3.

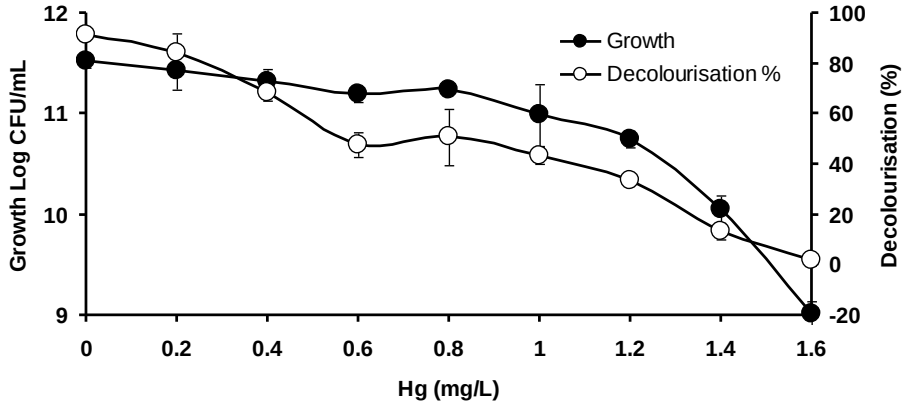

Figure 4. Growth of the inoculum and decolorization of 200 ppm of RR120 under different mercury concentrations after 24 h of incubation. Data points represent mean ± SD, n=3.

3.5. Effect of chromium on the decolorization of Reactive Red 120 by consortium JR3

Chromium was found to have the weakest effect on the decolorization ability of consortium JR3. The extent of tolerance capability was investigated in this study. Increasing chromium concentration results in less decolorization of RR120 and a lower consortium growth rate (Figure 5). A concentration of 1 ppm to 3 ppm of Cr results in an average of 75% decolorization activity. There is no significant difference between these concentrations (P>0.005). An increase beyond 10 ppm results in a significant drop in decolorization. Additionally, 7 ppm of Cr reduced decolorization by 54.7%, with consortium growth at 11.13 log CFU. Consortium JR3 was able to tolerate up to 15 ppm of Cr concentration; however, the decolorization reduced by 90%, suggesting an increase beyond this concentration will result in total inhibition.

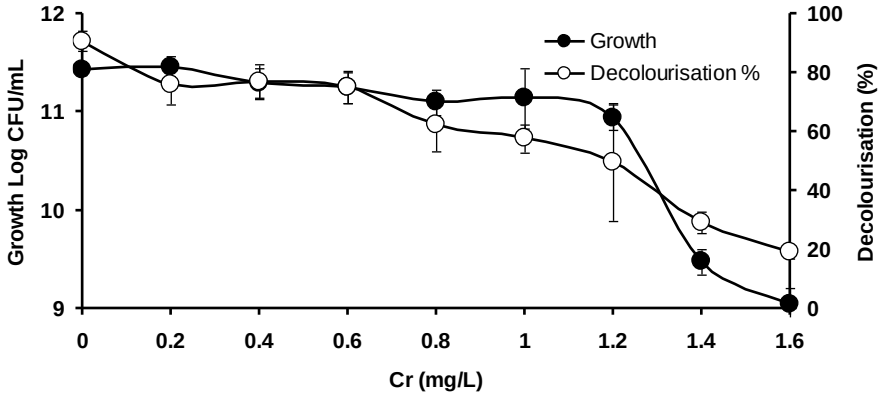

Figure 5. Growth of the inoculum and decolorization of 200 ppm RR120 under different chromium concentrations after 24 h of incubation. Data points represent mean ± SD, n=3.

3.6. Inhibition kinetics of chromium on consortium JR3 ability to decolorize Reactive Red 120

The effects of various kinetics models fitted based on different concentrations of chromium on the decolorization rate of RR120 by consortium JR3 is interpreted in Figure 6. The correlation coefficient value (R^2) for the RR120 Levenspiel reduction model was 0.98, illustrating a good fit with the actual data, followed by the Shukor model, with an R^2 value of 0.97 (Table 6). Another important indicator for allocating the perfect match between the expected and experimental results is the BF. When dealing with microbial azo dye decolonization, a BF value of <1 represents a fail-dangerous model, while a value of >1 indicates a fail-safe model. Besides that, the AF should be ≥1, and any higher value indicates a fail-safe model. Based on these requirements, the Levenspiel model fits a good model, with a BF value of 1.00 and an AF value of 1.02. Moreover, the lowest AICc in the Levenspiel model indicates a less preferrable model compared to the rest of the models. According to the best model, Levenspiel recorded a maximum RR120 reduction rate (μ_{max}) of 0.632 h^{-1}, while the saturation constant (K_c) and inhibitory constant (m) were 15.08% and 0.5783%, respectively.

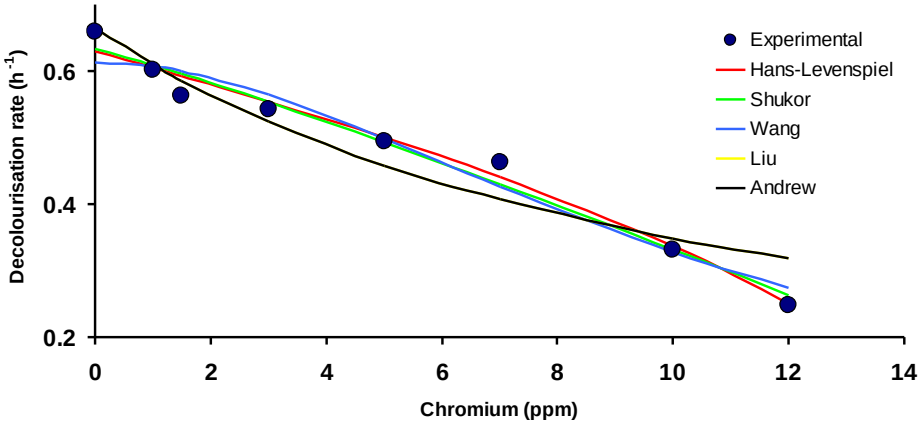

Figure 6. RR120 decolorization rate by consortium JR3 plotted against the various concentrations of chromium, as modeled according to the Wang model, Liu model, Shukor model and Andrews model.

Table 6. Statistical analysis of the kinetics models for heavy metal inhibition, with focus on chromium for consortium JR3. The BF and AF values are unavailable for the Andrews model due to the model plot failure.

	Levenspiel	Shukor	Wang	Liu	Andrews
R^2	0.98	0.97	0.97	0.96	0.0
Adjusted R^2	0.98	0.96	0.95	0.92	0.0
AICc	–57.85	–55.91	–50.9085	–50.64	–16.64
BIC	–62.17	–60.23	–55.23	–51.23	–20.97
HQC	–62.79	–60.85	–55.84	–51.85	–21.58
BF	1.00	1.00	1.01	1.01	NA
AF	1.02	1.04	1.05	1.07	NA

4. Discussion

An essential aspect of bioremediation is the correlation between a microbial population's specific growth rate (μ) and the substrate (RR120) concentration (S). The association defines a class of rate rules known as theoretical models that are based on empirical data. These simulations are merely numerical formulas meant to characterize a system's behavior. The estimations of these parameters suggest that the Aiba model best describes the inhibition kinetics of consortium JR3's cell growth.

There are limited data on the RR120 decolorization and utilization kinetics by microorganisms in the literature, which provides a good opportunity to study its growth kinetics. Most of the studies concerning substrate inhibition on microbial growth were done with focus on phenol [41], molybdenum [39], hydrocarbons [42,43] and copper [44], but none focusing on RR120 azo dye to date. Previous studies on other xenobiotics, such as molybdenum reduction by *Bacillus* sp. A.rzi, indicated that Luong developed the best model, followed by Haldane and Monod [45]. Meanwhile, in the area of pyrene degradation by *E. cloacae* BT, the Luong model was best fitted with a μ_{max} value of 0.032 h^{-1} at a concentration of 200 ppm. *Acinetobacter johnsonii* was reported to have Aiba as the best model, with a μ_{max} value of 0.537 h^{-1} for the excess effect of nitrogen concentration [46]. Aiba was the best-fitting secondary model of acrylamide substrate inhibition for *Pseudomonas* sp. [47], chromium

substrate inhibition for *Serratia* sp. [48] and molybdenum substrate inhibition for *Enterobacter* sp. [49].

However, this is the first paper to report Aiba as the best model in a combination of mixed bacterial strains containing *Pseudomonas aeruginosa*, *Serratia marcescens* and *Enterobacter sp*. in RR120, which follows previously reported individual strains [47,49]. Although the consortium JR3 was able to decolorize RR120 at more than 400 ppm, increasing the concentration beyond 200 or 400 ppm was found to be inhibitory to the specific growth. The drastic fall in specific growth rate from 0.795 to 0.445 h^{-1} for 100 ppm to 300 ppm and 0.279 to 0.103 h^{-1} for 400 to 600 ppm, respectively, was because of a prolonged lag time at those concentrations and the growth inhibition induced by the toxicant utilized in the investigation. The behavior can be explained by the lack of co-substrate needed to overcome RR120 saturation in consortium JR3. Although adding more co-substrate could solve the shortened lag phase at higher concentrations, this might lead to consortium JR3 utilizing the co-substrate as an alternate carbon source.

The ability of the consortium to decolorize RR120 in the presence of heavy metals provided valuable insight into its ability to remediate toxic effluents. Juru River not only accommodates textile industries, but it also houses various heavy machinery industries along the riverside. Due to anthropogenic activity, untreated waste from this kind of industry is being released into the river. Under this condition, those native bacteria to the sites are not only exposed to dye waste, but also to industrial waste containing heavy metals. For instance, one of the earliest studies [50] discovered traces of Cu, Pb, Zn, Mn and Fe in Juru River sediments. Moreover, Zn, Cu, Pb and Cd were also found in clams and fish caught in that river [51].

The presence of mercury and lead at concentrations of 18.46 mg L^{-1} and 0.04 mg L^{-1}, respectively, complicates the situation further. The situation is already worsened with poor dissolved oxygen levels [52]. Both studies show that there is a positive correlation between the presence of heavy metals in the river and at industrial sites, as the number of pollutants increases with the rapid development of heavy machinery factories. To make matters worse, this has been happening for the past 20 years. In this case, the surrounding environmental conditions influence consortium JR3 in terms of heavy metals tolerance. Repeated exposure has allowed those native bacteria to acclimatize to new conditions.

Second, microbial survival in polluted environments varies according to inherent structural, biochemical and physiological properties with gene adaption [53–55]. Prolonged exposure to heavy metals contaminates, and the bacteria have developed appropriate mechanisms for survivability. Since consortium JR3 consists of *Serratia* sp., *Pseudomonas* sp. and *Enterobacter* sp., each of these individual strains has its unique mechanism to cope with heavy metal toxicity. The five main mechanisms against heavy metals are extracellular sequestration, an extracellular barrier, intracellular sequestration, the active transport of metal ions and the reduction of metal ions [56].

Uniquely, many genes responsible for heavy metal tolerance are naturally found in some bacteria before exposure, suggesting that acquired tolerance is a strain's ability to be further enhanced. As reported in one paper [57], three genes encoding Cd/Pb/Hg/Zn-transporting ATPase, as well as three putative genes encoding the Zn/Co/Cd resistance protein CzcD, are naturally present in *Serratia marcescens* isolated from roots of *Solanum nigrum*. Although this bacterium had no previous exposure to heavy metals, the strain developed tolerance when exposed to Cd. The findings [57] are further supported by the work of Kotoky et al. [58], where *Serratia marcescens* was found to be highly resistant to Cd by utilizing the glutathione-S-transferase mechanism for detoxification [58]. There are similarities between the attitudes expressed by consortium JR3 in this study and those described by

Khan et al. [57]. The ability to decolorize RR120 in the presence of cadmium can probably be attributed to the *Serratia marcescens* strain MM06, as this genus is known for its metal-tolerant capability due to the presence of metal-efflux genes [59]. In addition, *Pseudomonas* sp. showed high resistance to heavy metals, antibiotics, detergents and organic solvents [60–63]. The CadR in *Pseudomonas* spp. is responsible for encoding a transcriptional regulatory protein that responds to $Cd(II) \gg Zn(II) > Hg(II)$ [64–66]. This function allows *Pseudomonas aeruginosa* strains in general to tolerate heavy metals. The novelty of consortium JR3 is its ability to withstand a large amount of chromium while maintaining a significant decolorization rate of RR120. This ability is rarely seen in other bacteria, yet achieving total decolorization at 10 ppm of chromium alone is a valuable asset in the bioremediation field. The inhibitory effect of chromium on dye biodegradation is discussed in [67], with the simultaneous removal of 100 ppm of mixed dyes consisting of RR120, Reactive Blue 5, Reactive Yellow 2 and Reactive Orange 16, with 25 ppm of hexavalent chromium resulting in 76.6–98.7% decolorization and 51.9–91.1% reduction, respectively, by *Pseudomonas aeruginosa* ZM120 after 180 h incubation under static conditions. Zhuang et al. observed a significant reduction in Direct Blue 2 decolorization in *Enterobacter faecalis* ST5, *Clostridium bifermentans* ST12 and *Oceanimonas smirnovii* ST3 when exposed to 1 ppm of lead and cadmium [68]. However, *Pseudomonas aeruginosa* HF5 had a negligible impact on the decolorization of RR120 when supplemented with lead, and it was able to achieve complete decolorization (>95%) even at 100 ppm of lead [69]. According to Hafeez et al., *Pseudomonas aeruginosa* was the best strain among 80 others able to tolerate a high concentration of lead [69].

The effect of mercury on RR120 decolorization has a distinct effect on consortium JR3. Normally, throughout the study, the observed medium slowly loses color from red to yellowish, indicating that consortium JR3 is consuming the dye; hence, decolorization has occurred. However, when exposed to mercury, the observed color change was different. After 48 h of incubation, the medium turned a green color at a mercury concentration of 0.1 ppm, while increasing the concentration to 1 ppm resulted in it remaining red (data not shown). Resulting in medium color change is a consequence of bacterial pigmentation induced by consortium JR3.

Mercury is highly toxic to living cells due to its strong affinity for the thiol groups of proteins. This could result in damage to the cells' protein channels, causing the bacteria to slowly die of starvation. To overcome this barrier, some species of *Pseudomonas* produce pyocyanin, particularly for iron metabolism [70,71]. This could explain why the culture medium turned green due to *Pseudomonas*' pyocyanin. Another possible explanation is the effect of the strains competing for the same source of nutrients. Consortium JR3 consists of *Pseudomonas aeruginosa*, *Serratia marcescens* and *Enterobacter* sp. Due to the presence of mercury, these strains are under huge stress and unable to consume and multiply efficiently. Thus, to increase the odds of survival, *Pseudomonas aeruginosa* releases pyocyanin, which is known to inhibit the growth of other organisms [72,73]. Pyocyanin is a secondary metabolite with the ability to oxidize and reduce other molecules and, therefore, kill microbes competing against *Pseudomonas aeruginosa* [73].

The cytotoxicity effect of mercury in *Serratia marcescens* results in the production of prodigiosin, which allows the bacteria to neutralize the mercury effect [58]. Furthermore, this effect was observed at 0.3 ppm onward. As the mercury concentration increases, red pigmentation increases with it. This observation can be explained by the findings in [74], which reported prodigiosin functions to convert toxic metabolites into the innocuous end product. The authors of [75] observed the red pigmentation to be correlated with an increased rate of ATP production during the population lag phase. During this

time, the pigmented cells of *Serratia marcescens* were able to accumulate ATP more rapidly and proliferate much faster [75,76]. At higher concentrations, most likely both *Pseudomonas aeruginosa* and *Enterobacter* sp. did not survive, leaving *Serratia marcescens* to proliferate much better, with no competition with either bacteria. However, with a lack of a synergistic effect of both species, *Serratia marcescens* produces prodigiosin to gain what is lost. Under this condition, *Serratia marcescens* strain MM06 seeks for an abundant energy source that is available from RR120. The ability of consortium JR3 to withstand up to 1.2 ppm of mercury is an added value, as most bacteria fail to do so. With the limited number of bacteria, the family is known to resist mercury toxicity, so finding one is extremely valuable in the bioremediation field. Mercury-resistant bacteria have been described for many phyla, including those of Actinobacteria, Firmicutes and Proteobacteria [77,78]. A handful of these organisms are capable of reducing Hg(II) to Hg(0) and/or degrading methylmercury, or simply resisting it [79,80]. Nevertheless, the ability of bacteria or a consortium to decolorize RR120 in the presence of mercury has not been reported before. Repeated exposure to industrial waste allows this native bacterium to adapt and tolerate it much better. Hence, applying the consortium JR3 to textile effluents consisting of heavy metals, especially mercury, will likely result in red pigmentation due to prodigiosin activity. This is where consortium JR3 shines compared to the rest of the known dye decoloring strains. The versatility of these strains could be a key changer in bioremediation application, not only because it is able to consume RR120 as the sole carbon source, but also because its tolerance toward various heavy metals provides a good solution for textile effluent treatment.

5. Conclusion

This study illustrates the ability of consortium JR3, which is comprised of *Pseudomonas aeruginosa* MM01, *Enterobacter* sp. MM05 and *Serratia marcescens* MM06, which were previously isolated from Juru River, Malaysia, to decolorize up to 700 ppm of RR120 and tolerate various heavy metal types. Discriminatory statistical analysis in modeling studies illustrates that the best growth kinetic model is the Aiba model. The consortium JR3 was able to decolorize RR120 in the presence of heavy metals such as silver, arsenic, cadmium, chromium, copper, mercury, lead and zinc. It was found that chromium had the weakest effect on RR120 decolorization, followed by zinc and lead. Meanwhile, mercury has the highest inhibitory effect on consortium JR3. In terms of chromium inhibition kinetics, the Levenspiel model had the best fit. A strain which displays heavy metal tolerance and dye-decolorizing ability is sought after, particularly for bioremediation.

Author Contributions

Conceptualization, M.Y.A.S and M.M..; methodology, M.Y.A.S. and M.M; software, M.M. and M.I.E.H.; validation, M.Y.AS., N.A.Y, B.G. and A.R.O; writing—original draft preparation, M.Y.A.S. and M.M.; writing—review and editing, M.M and M.Y.A.S.; supervision, M.Y.A.S., N.A.Y. M.I.E.H., A.R.O. and B.G

Data Availability Statement

The data presented in this study are openly available at FigShare.com, https://doi.org/10.6084/m9.figshare.22094810.v1.

Conflicts of Interest

We declare no competing financial interests.

References

1. Arora J, Agarwal P, Gupta G (2017) Rainbow of Natural Dyes on Textiles Using Plants Extracts: Sustainable and Eco-Friendly Processes. *Green Sustain Chem* 7: 35–47. https://doi.org/10.4236/gsc.2017.71003
2. Ding Y, Freeman HS (2017) Mordant dye application on cotton: optimisation and combination with natural dyes. *Color Technol* 133: 369–375. https://doi.org/10.1111/cote.12288
3. Jensen B, Evans RP, Tata G, et al. (2019) They'll Never Be Royals: The "Purple" Textiles of Fag el-Gamous. *Excavations at the Seila Pyramid and Fag el-Gamous Cemetery* 207–248. https://doi.org/10.1163/9789004416383_011
4. Merdan N, Eyupoglu S, Duman MN (2017) Ecological and Sustainable Natural Dyes, In: Muthu SS (Ed.), *Textiles and Clothing Sustainability: Sustainable Textile Chemical Processes* Singapore, Springer, 1–41. https://doi.org/10.1007/978-981-10-2185-5_1
5. Gupta VK (2019) Fundamentals of Natural Dyes and Its Application on Textile Substrates, IntechOpen.
6. Khattab TA, Abdelrahman MS, Rehan M (2020) Textile dyeing industry: environmental impacts and remediation. *Environ Sci Pollut Res Int* 27: 3803–3818. https://doi.org/10.1007/s11356-019-07137-z
7. Raval NP, Shah PU, Shah NK (2016) Adsorptive amputation of hazardous azo dye Congo red from wastewater: a critical review. *Environ Sci Pollut Res* 23: 14810–14853. https://doi.org/10.1007/s11356-016-6970-0
8. Singh RL, Singh PK, Singh RP (2015) Enzymatic decolorization and degradation of azo dyes – A review. *Int Biodeter Biodegr* 104: 21–31. https://doi.org/10.1016/j.ibiod.2015.04.027
9. Yan LKQ, Fung KY, Ng KM (2018) Aerobic sludge granulation for simultaneous anaerobic decolorization and aerobic aromatic amines mineralization for azo dye wastewater treatment. *Environ Technol* 39: 1368–1375. https://doi.org/10.1080/09593330.2017.1329354
10. Balapure K, Bhatt N, Madamwar D (2015) Mineralization of reactive azo dyes present in simulated textile waste water using down flow microaerophilic fixed film bioreactor. *Bioresource Technol* 175: 1–7. https://doi.org/10.1016/j.biortech.2014.10.040
11. Gürses A, Açıkyıldız M, Güneş K, et al. (2016) Classification of Dye and Pigments, In: Gürses A, Açıkyıldız M, Güneş K, et al. (Eds.), *Dyes Pigments*, Cham, Springer International Publishing, 31–45. https://doi.org/10.1007/978-3-319-33892-7_3
12. Pang YL, Abdullah AZ (2013) Current Status of Textile Industry Wastewater Management and Research Progress in Malaysia: A Review. *CLEAN – Soil, Air, Water* 41: 751–764. https://doi.org/10.1002/clen.201000318
13. Rawat D, Mishra V, Sharma RS (2016) Detoxification of azo dyes in the context of environmental processes. *Chemosphere* 155: 591–605. https://doi.org/10.1016/j.chemosphere.2016.04.068
14. Hussain G, Ather M, Khan MUA, et al. (2016) Synthesis and characterization of chromium (III), iron (II), copper (II) complexes of 4-amino-1-(p-sulphophenyl)-3-methyl-5-pyrazolone based acid dyes and their applications on leather. *Dyes Pigments* 130: 90–98. https://doi.org/10.1016/j.dyepig.2016.02.014

15. Rawat D, Sharma RS, Karmakar S, et al. (2018) Ecotoxic potential of a presumably non-toxic azo dye. *Ecotoxicology and Environmental Safety* 148: 528–537. https://doi.org/10.1016/j.ecoenv.2017.10.049
16. Sarkar S, Banerjee A, Halder U, et al. (2017) Degradation of Synthetic Azo Dyes of Textile Industry: a Sustainable Approach Using Microbial Enzymes. *Water Conserv Sci Eng* 2: 121–131. https://doi.org/10.1007/s41101-017-0031-5
17. Manogaran M, Yasid NA, Othman AR, et al. (2021) Biodecolourisation of Reactive Red 120 as a Sole Carbon Source by a Bacterial Consortium—Toxicity Assessment and Statistical Optimisation. *International Journal of Environmental Research and Public Health* 18: 2424. https://doi.org/10.3390/ijerph18052424
18. Brilon C, Beckmann W, Hellwig M, et al. (1981) Enrichment and Isolation of Naphthalenesulfonic Acid-Utilizing Pseudomonads. *Appl Environ Microbiol* 42: 39–43. https://doi.org/10.1128/aem.42.1.39-43.1981
19. Zhu H, Yang J, Xiaowei C (2019) Application of Modified Gompertz Model to Study on Biogas production from middle temperature co-digestion of pig manure and dead pigs. *E3S Web Conf* 118: 03022. https://doi.org/10.1051/e3sconf/201911803022
20. Yahuza S, Dan-Iya BI, Sabo IA (2020) Modelling the Growth of Enterobacter sp. on Polyethylene. *J Biochem Microbiol Biotechn* 8: 42–46. https://doi.org/10.54987/jobimb.v8i1.508
21. Abubakar A, Ibrahim S, Abba M (2021) Mathematical Modelling of Azo Blue Dye Degradation by Streptomyces DJP15. *Bull of Environ Sci Sustain Manage* 5: 27–31. https://doi.org/10.54987/bessm.v5i1.588
22. Ibrahim S, Abdulrasheed M, Ibrahim H, et al. (2021) Mathematical Modelling of the Growth of Yeast Candida tropicalis TL-F1 on Azo Dyes. *J Biochem Microbiol Biotechn* 9: 43–47. https://doi.org/10.54987/jobimb.v9i1.575
23. Uba G, Yakubu A, Baba AM (2021) The Effect of the plant Adiantum philippense Extracts on Biofilms Formation and Adhesion to Shigella flexneri: A Predictive Modelling Approach. *J Biochem Microbiol Biotechn* 9: 34–39. https://doi.org/10.54987/jobimb.v9i2.615
24. Yahuza S, Sabo IA (2021) Mathematical Modelling of the Growth of *Bacillus cereus* Strain wwcp1on Malachite Green Dye. *J Biochem Microbiol Biotechn* 9: 25–29. https://doi.org/10.54987/jobimb.v9i2.613
25. Yano T, Koga S (1969) Dynamic Behavior of the Chemostat Subject. XI: 139–153. https://doi.org/10.1002/bit.260110204
26. Aiba S, Shoda M, Nagatani M (1968) Kinetics of product inhibition in alcohol fermentation. *Biotechnol Bioeng* 10: 845–864. https://doi.org/10.1002/bit.260100610
27. Haldane JBS (1930) Enzymes, Longmans, Green and Co. London.
28. Teissier G (1942) Growth of bacterial populations and the available substrate concentration. *Rev Sci Instrum* 3208: 209–214.
29. Monod J (1949) a Certain Number. *Annual Reviews in M* 3: 371–394. https://doi.org/10.1146/annurev.mi.03.100149.002103
30. Wang J, Wan W (2009) Kinetic models for fermentative hydrogen production: A review. *Int J Hydrogen Energ* 34: 3313–3323. https://doi.org/10.1016/j.ijhydene.2009.02.031
31. Wang Y, Zhao Q-B, Mu Y, et al. (2008) Biohydrogen production with mixed anaerobic cultures in the presence of high-concentration acetate. *Int J Hydrogen Energ* 33: 1164–1171. https://doi.org/10.1016/j.ijhydene.2007.12.018

32. Liu Y (2006) A simple thermodynamic approach for derivation of a general Monod equation for microbial growth. *Biochem Eng J* 31: 102–105. https://doi.org/10.1016/j.bej.2006.05.022
33. Andrews JF (1968) A mathematical model for the continuous culture of microorganisms utilizing inhibitory substrates. *Biotechnol Bioeng* 10: 707–723. https://doi.org/10.1002/bit.260100602
34. Manogaran M, Othman AR, Shukor MY, et al. (2019) Modelling the Effect of Heavy Metal on the Growth Rate of an SDS-degrading Pseudomonas sp. strain DRY15 from Antarctic soil. *Bioremediat Sci Technol Res* 7: 41–45. https://doi.org/10.54987/bstr.v7i1.463
35. Wayman M, Tseng MC (1976) Inhibition-threshold substrate concentrations. *Biotechnol Bioeng* 18: 383–387. https://doi.org/10.1002/bit.260180308
36. Głuszcz P, Petera J, Ledakowicz S (2011) Mathematical modeling of the integrated process of mercury bioremediation in the industrial bioreactor. *Bioproc Biosyst Eng* 34: 275–285. https://doi.org/10.1007/s00449-010-0469-8
37. Abubakar A, Uba G, Biu HA (2021) Kinetics Modelling of Pseudomonas stutzeri strain DN2 Growth Behaviour in Tributyltin Chloride. *J Environ Microbiol Toxicol* 9: 13–18. https://doi.org/10.54987/jemat.v9i2.641
38. Yakasai HM, Babandi A, Manogaran M (2020) Modelling the Kinetics Molybdenum Reduction Rate by *Morganella* sp. *J Environ Microbiol Toxicol* 8: 18–23. https://doi.org/10.54987/jemat.v9i2.641
39. Halmi MIE, Abdullah SRS, Johari WLW, et al. (2016) Modelling the kinetics of hexavalent molybdenum (Mo6+) reduction by the Serratia sp. strain MIE2 in batch culture. *Rend Fis Acc Lincei* 27: 653–663. https://doi.org/10.1007/s12210-016-0545-3
40. Akaike H (1987) Factor analysis and AIC. *Psychometrika* 52: 317–332. https://doi.org/10.1007/BF02294359
41. Ahmad SA, Shamaan NA, Arif NM, et al. (2012) Enhanced phenol degradation by immobilized Acinetobacter sp. strain AQ5NOL 1. *World J Microbiol Biotechnol* 28: 347–352. https://doi.org/10.1007/s11274-011-0826-z
42. Fernández EL, Merlo EM, Mayor LR, et al. (2016) Kinetic modelling of a diesel-polluted clayey soil bioremediation process. *Sci Total Environ* 557–558: 276–284. https://doi.org/10.1016/j.scitotenv.2016.03.074
43. Nwankwegu AS, Li Y, Jiang L, et al. (2020) Kinetic modelling of total petroleum hydrocarbon in spent lubricating petroleum oil impacted soil under different treatments. *null* 41: 339–348. https://doi.org/10.1080/09593330.2018.1498543
44. Baltazar M dos PG, Gracioso LH, Avanzi IR, et al. (2019) Copper biosorption by Rhodococcus erythropolis isolated from the Sossego Mine – PA – Brazil. *J Mater Res Technol* 8: 475–483. https://doi.org/10.1016/j.jmrt.2018.04.006
45. Othman AR, Bakar NA, Halmi MIE, et al. (2013) Kinetics of Molybdenum Reduction to Molybdenum Blue by Bacillus sp. Strain A.rzi. *BioMed Res Int* 2013: e371058. https://doi.org/10.1155/2013/371058
46. Zhang Y, Wang X, Wang W, et al. (2019) Investigation of growth kinetics and partial denitrification performance in strain Acinetobacter johnsonii under different environmental conditions. *Roy Soc Open Sci* 6: 191275. https://doi.org/10.1098/rsos.191275
47. Abubakar A, Gusmanizar N, Rusnam M, et al. (2020) Remodelling the Growth Inhibition Kinetics of Pseudomonas sp. Strain DrY Kertih on Acrylamide. *Bioremediat Sci Technol Res* 8: 16–20. https://doi.org/10.54987/bstr.v8i2.553

48. Upadhyay S, Tarafdar A, Sinha A (2020) Assessment of Serratia sp. isolated from iron ore mine in hexavalent chromium reduction: kinetics, fate and variation in cellular morphology. *Environ Technol* 41: 1117–1126. https://doi.org/10.1080/09593330.2018.1521875
49. Yakasai HM, Babandi A, Ibrahim S (2020) Modelling the Inhibition Kinetics of Molybdenum Reduction by the Molybdate-reducing Enterobacter cloacae. *Bull Environ Sci Sustain Manage* 4: 11–17. https://doi.org/10.54987/bessm.v4i2.560
50. Lim P-E, Kiu M-Y (1995) Determination and speciation of heavy metals in sediments of the Juru River, Penang, Malaysia. *Environ Monit Assess* 35: 85–95. https://doi.org/10.1007/BF00633708
51. Idriss AA, Ahmad AK (2015) Heavy Metal Concentrations in Fishes from Juru River, Estimation of the Health Risk. *Bull Environ Contam Toxicol* 94: 204–208. https://doi.org/10.1007/s00128-014-1452-x
52. Nurlizah Abu Bakar, Ahmad Razi Othman, Mohd Yunus Shukor (2019) Heavy metals detection from contaminated river using molybdenum reducing enzyme. *J Kejuruter* 31: 303–308. https://doi.org/10.17576/jkukm-2019-31(2)-15
53. Hu X, Qiao Y, Chen L-Q, et al. (2019) Enhancement of solubilization and biodegradation of petroleum by biosurfactant from Rhodococcus erythropolis HX-2. *Geomicrobiol J* https://doi.org/10.1080/01490451.2019.1678702
54. Dauda DM, Emere MC, Umar Y, et al. (2021) Effects of Kaduna Refining and Petrochemical Corporation Effluents on the Abundance and Distribution of Phytoplankton Community along River Rido, Kaduna, Nigeria. *J Environ Bioremediat Toxicol* 4: 17–22. https://doi.org/10.54987/jebat.v4i2.628
55. Gafar AA, Shukor MY (2018) Characterisation of an acrylamide-degrading bacterium and its degradation pathway. *J Environ Microbiol Toxicol* 6: 29–33. https://doi.org/10.54987/jemat.v6i2.441
56. Nyika JM (2021) Recent Advancements in Bioremediation of Metal Contaminants, Tolerance of Microorganisms to Heavy Metals, 2021. Available from: www.igi-global.com/chapter/tolerance-of-microorganisms-to-heavy-metals/259564. https://doi.org/10.4018/978-1-7998-4888-2.ch002
57. Khan AR, Park G-S, Asaf S, et al. (2017) Complete genome analysis of Serratia marcescens RSC-14: A plant growth-promoting bacterium that alleviates cadmium stress in host plants. *PLOS ONE* 12: e0171534. https://doi.org/10.1371/journal.pone.0171534
58. Kotoky R, Nath S, Kumar Maheshwari D, et al. (2019) Cadmium resistant plant growth promoting rhizobacteria Serratia marcescens S2I7 associated with the growth promotion of rice plant. *Environ Sustain* 2: 135–144. https://doi.org/10.1007/s42398-019-00055-3
59. dos Reis Ferreira GM, Pires JF, Ribeiro LS, et al. (2023) Impact of lead (Pb2+) on the growth and biological activity of Serratia marcescens selected for wastewater treatment and identification of its zntR gene—a metal efflux regulator. *World J Microbiol Biotechnol* 39: 91. https://doi.org/10.1007/s11274-023-03535-1
60. Puzari M, Chetia P (2017) RND efflux pump mediated antibiotic resistance in Gram-negative bacteria Escherichia coli and Pseudomonas aeruginosa: a major issue worldwide. *World J Microbiol Biotechnol* 33: 24. https://doi.org/10.1007/s11274-016-2190-5
61. Chellaiah ER (2018) Cadmium (heavy metals) bioremediation by Pseudomonas aeruginosa: a minireview. *Appl Water Sci* 8: 154. https://doi.org/10.1007/s13201-018-0796-5

62. Devi R, Nampoothiri KM, Sukumaran RK, et al. (2020) Lipase of Pseudomonas guariconesis as an additive in laundry detergents and transesterification biocatalysts. *J Basic Microb* 60: 112–125. https://doi.org/10.1002/jobm.201900326
63. Nordin N, Zakaria MR, Halmi MIE, et al. (2013) Isolation and screening of high efficiency biosurfactant-producing bacteria Pseudomonas sp. *J Biochem Microbiol Biotechn* 1: 25–31. https://doi.org/10.54987/jobimb.v1i1.381
64. Prabhakaran R, Rajkumar SN, Ramprasath T, et al. (2018) Identification of promoter PcadR, in silico characterization of cadmium resistant gene cadR and molecular cloning of promoter PcadR from Pseudomonas aeruginosa BC15. *Toxicol Ind Health* 34: 819–833. https://doi.org/10.1177/0748233718795934
65. Tang X, Zeng G, Fan C, et al. (2018) Chromosomal expression of CadR on Pseudomonas aeruginosa for the removal of Cd(II) from aqueous solutions. *Sci Total Environ* 636: 1355–1361. https://doi.org/10.1016/j.scitotenv.2018.04.229
66. Cayron J, Effantin G, Prudent E, et al. (2020) Original sequence divergence among Pseudomonas putida CadRs drive specificity. *Res Microbiol* 171: 21–27. https://doi.org/10.1016/j.resmic.2019.11.001
67. Maqbool Z, Hussain S, Ahmad T, et al. (2016) Use of RSM modeling for optimizing decolorization of simulated textile wastewater by Pseudomonas aeruginosa strain ZM130 capable of simultaneous removal of reactive dyes and hexavalent chromium. *Environ Sci Pollut Res* 23: 11224–11239. https://doi.org/10.1007/s11356-016-6275-3
68. Zhuang M, Sanganyado E, Zhang X, et al. (2020) Azo dye degrading bacteria tolerant to extreme conditions inhabit nearshore ecosystems: Optimization and degradation pathways. *J Environ Manage* 261: 110222. https://doi.org/10.1016/j.jenvman.2020.110222
69. Hafeez F, Farheen H, Mahmood F, et al. (2018) Isolation and characterization of a lead (Pb) tolerant Pseudomonas aeruginosa strain HF5 for decolorization of reactive red-120 and other azo dyes. *Ann Microbiol* 68: 943–952. https://doi.org/10.1007/s13213-018-1403-6
70. Elkhawaga AA, Khalifa MM, El-badawy O, et al. (2019) Rapid and highly sensitive detection of pyocyanin biomarker in different Pseudomonas aeruginosa infections using gold nanoparticles modified sensor. *PLOS ONE* 14: e0216438. https://doi.org/10.1371/journal.pone.0216438
71. Saunders SH, Tse ECM, Yates MD, et al. (2020) Extracellular DNA Promotes Efficient Extracellular Electron Transfer by Pyocyanin in Pseudomonas aeruginosa Biofilms. *Cell* 182: 919-932.e19. https://doi.org/10.1016/j.cell.2020.07.006
72. El Feghali PAR, Nawas T (2018) Extraction and purification of pyocyanin: a simpler and more reliable method. *MOJ Toxicology* 4: 417–422. https://doi.org/10.15406/mojt.2018.04.00139
73. Qasim DA (2019) Molecular detection of pseudomonas aeruginosa isolated from minced meat and studies the pyocyanin effectiveness on pathogenic bacteria. *Iraqi J Agric Sci* 50. https://doi.org/10.36103/ijas.v50i4.764
74. Lin S-R, Lin C-S, Chen C-C, et al. (2020) Doxorubicin metabolism moderately attributes to putative toxicity in prodigiosin/doxorubicin synergism in vitro cells. *Mol Cell Biochem* 475: 119–126. https://doi.org/10.1007/s11010-020-03864-x
75. Haddix PL, Shanks RMQ (2018) Prodigiosin pigment of Serratia marcescens is associated with increased biomass production. *Arch Microbiol* 200: 989–999. https://doi.org/10.1007/s00203-018-1508-0

76. Haddix PL, Shanks RMQ (2020) Production of prodigiosin pigment by Serratia marcescens is negatively associated with cellular ATP levels during high-rate, low-cell-density growth. *Can J Microbiol* https://doi.org/10.1139/cjm-2019-0548
77. Mello IS, Pietro-Souza W, Barros BM, et al. (2019) Endophytic bacteria mitigate mercury toxicity to host plants. *Symbiosis* 79: 251–262. https://doi.org/10.1007/s13199-019-00644-0
78. Yan C, Wang F, Liu H, et al. (2020) Deciphering the toxic effects of metals in gold mining area: Microbial community tolerance mechanism and change of antibiotic resistance genes. *Environ Res* 189: 109869. https://doi.org/10.1016/j.envres.2020.109869
79. Imron MF, Kurniawan SB, Soegianto A (2019) Characterization of mercury-reducing potential bacteria isolated from Keputih non-active sanitary landfill leachate, Surabaya, Indonesia under different saline conditions. *J Environ Manage* 241: 113–122. https://doi.org/10.1016/j.jenvman.2019.04.017
80. Mello IS, Targanski S, Pietro-Souza W, et al. (2020) Endophytic bacteria stimulate mercury phytoremediation by modulating its bioaccumulation and volatilization. *Ecotox Environ Safe* 202: 110818. https://doi.org/10.1016/j.ecoenv.2020.110818

AIMS Press